JOURNAL OF GEOPHYSICAL RESEARCH, VOL. 114, D10302, doi:10.1029/2008JD011374, 2009

Tropospheric intrusions associated with the secondary tropopause

L. L. Pan,[1] W. J. Randel,[1] J. C. Gille,[1] W. D. Hall,[1] B. Nardi,[1] S. Massie,[1] V. Yudin,[1] R. Khosravi,[1] P. Konopka,[2] and D. Tarasick[3]

Received 29 October 2008; revised 6 March 2009; accepted 18 March 2009; published 20 May 2009.

[1] Deep intrusions of tropospheric air into the lower stratosphere above the subtropical jet are investigated using new observations and meteorological analyses. These intrusions are characterized by low ozone concentration and low static stability. The low-ozone layer is consistently observed from ozonesonde profiles and satellite remote sensing data from Aura/HIRDLS. The intruding layer occurs along and under the poleward extending tropical tropopause, which becomes the secondary tropopause in middle to high latitudes. The association of the ozone and the thermal structure provides evidence for the physical significance of the subtropical tropopause break and the secondary tropopause. The core of the intruding layer is typically between 370 and 400 K potential temperature (~15 km), but the vertical extent of the intrusion can impact ozone above 400 K, the lower boundary of the overworld. Two intrusion events over the continental United States in the spring of 2007 are analyzed to show the spatial extent and the temporal evolution of the intruding air mass. These examples demonstrate the effectiveness of potential temperature lapse rate, i.e., static stability, as a diagnostic for the intrusion event. Comparison with the potential vorticity field is made to show the complementarity of the two dynamical fields. The static stability diagnostic provides a tool to map out the horizontal extent of the intruding layer and to investigate its evolution. Furthermore, the diagnostic makes it possible to forecast the intrusion event for field studies.

Citation: Pan, L. L., W. J. Randel, J. C. Gille, W. D. Hall, B. Nardi, S. Massie, V. Yudin, R. Khosravi, P. Konopka, and D. Tarasick (2009), Tropospheric intrusions associated with the secondary tropopause, *J. Geophys. Res.*, *114*, D10302, doi:10.1029/2008JD011374.

1. Introduction

[2] Stratosphere-troposphere exchange (STE) plays a significant role in redistributing chemical constituents in the upper troposphere and lower stratosphere (UTLS). The distributions of ozone and water vapor in the UTLS are of particular interest, because these two trace gases make significant contributions to the radiative forcing. Their distributions and controlling mechanisms are important elements of chemistry-climate interaction.

[3] A global perspective of STE, based on the controlling processes, distinguishes between the region where the isentropes cross the tropopause, known as the "middleworld," and the region where the isentropes lie entirely in the stratosphere, known as the "overworld" [*Hoskins*, 1991]. The boundary of the two regions is approximately the 380–400 K potential temperature surface. The distinction between the two regions is significant, because tropospheric air mass enters the overworld primarily through the tropical tropopause, while the middleworld is strongly influenced by STE across the extratropical tropopause. Because isentropic motion occurs on a relatively short time scale, isentropic mixing in this region is a significant mechanism of STE, although it is challenging to quantify [*Holton et al.*, 1995].

[4] A related issue is the definition and characterization of the tropopause as a chemical transport boundary. It has long been recognized that the temperature lapse rate-based thermal definition produces breaks and multiple tropopauses in the extratropics [e.g., *Palmen and Newton*, 1969; *Kochanski*, 1955]. Recent analyses using radiosondes and high-resolution GPS temperature measurements have shown that the frequency of occurrence and areal extent of double tropopauses are much more extensive than previously realized [*Seidel and Randel*, 2006; *Schmidt et al.*, 2006; *Randel et al.*, 2007a]. It is not well understood whether the breaks and multiple tropopauses are physically meaningful or merely artifacts of the thermal lapse rate definition. An alternative definition of the tropopause using PV surfaces, often termed the dynamical tropopause, provides a single surface to separate the stratospheric and tropospheric air masses. Since PV is a quasi-conservative tracer for stratospheric air mass, the dynamical definition is often considered more physical [*Danielsen*, 1968; *Shapiro*, 1978; *Hoskins et al.*, 1985; *Holton et al.*, 1995].

[5] In this work, we present an analysis using newly available satellite data from the High Resolution Dynamics

[1] National Center for Atmospheric Research, Boulder, Colorado, USA.
[2] Forschungszentrum Jülich, Jülich, Germany.
[3] Experimental Studies, Air Quality Research Division, Environment Canada, Downsview, Ontario, Canada.

0148-0227/09/2008JD011374$09.00

Limb Sounder (HIRDLS) on Aura, combined with ozonesonde data and high-resolution meteorological analyses, to show connections between the existence of the tropopause break, the occurrence of the secondary tropopause and chemical transport via quasi-isentropic motion in the middleworld. We show that episodes of poleward transport (or intrusions) of subtropical air occur above the subtropical jet, bringing air with low ozone and low static stability to the region above the extratropical tropopause. The low-stability air results in the formation of a secondary tropopause, which becomes a poleward extension of the tropical tropopause (near 17 km). The vertical extent of these events can sometimes extend above the 400 K potential temperature surface, and the intrusion therefore can erode the bottom of the overworld.

[6] There has been a long history of observing laminated ozone structure in the lower stratosphere from ozonesondes. *Dobson* [1973] presented the first statistical analysis for the altitude of occurrence of laminae, and suggested that double tropopauses at midlatitudes were caused by tropospheric air entering the stratosphere at the subtropical tropopause break. A similar study by *Reid et al.* [2000] supported this origin with aircraft observations of water vapor and N_2O, and noted the potential effect of such intrusions on the total ozone column. Additional analyses of the ozone structure in the lower stratosphere have been made using ozonesonde data in recent years [*Lemoine*, 2004; *Hwang et al.*, 2007; *Randel et al.*, 2007a].

[7] Using HIRDLS ozone and HNO_3 data, *Olsen et al.* [2008] presented observations of a laminar structure in the midlatitude lower stratosphere and concluded that the structure was produced by intruding air mass from the tropical lower stratosphere. Their analyses showed that the structure and the evolution of this event were well reproduced by the Global Modeling Initiative chemical transport model using analyzed meteorological fields. They also discussed a possible relationship of the low ozone with the secondary tropopauses, but the structure was not examined in detail.

[8] The dynamical conditions during the occurrence of low-ozone layers have been investigated previously for several events over northern Europe using isentropic PV. The intruding low-ozone layer was identified as a poleward excursion of air from the region of the subtropical jet, as a result of Rossby wave breaking (RWB) [*Vaughan and Timmis*, 1998; *O'Connor et al.*, 1999]. The dynamics of RWB has been studied mostly for lower isentropes, typically below 350 K, the range around or below the subtropical jet core [e.g., *Peters and Waugh*, 1996]. The behavior of RWB for 370–400 K has not been examined extensively.

[9] The newly available satellite data allow examination of the structure and spatial extent of the intruding low-ozone layer as well as signatures in dynamical fields. One of the main objectives of this work is to present an effective diagnostic for this type of event using the potential temperature lapse rate ($\frac{\partial\theta}{\partial z}$), i.e., the static stability, in association with the double tropopauses. Using this diagnostic, we are able to map out the 3-D structure of the intrusion, as well as examine its temporal evolution. Further, this diagnostic shows the transport origin of the low-stability layer and provides an indication of how the associated dynamics alter the thermal structure of the lowermost stratosphere.

[10] The analyses will focus on two selected events over North America. These cases are used to examine the 3-D structure of the intrusion and associated meteorological conditions, to establish consistency between satellite, ground based measurements, and finally to investigate the dynamical evolution of the process.

2. Data Description

[11] Analyses in this work involve three data sets: ozone retrievals from satellite, ozonesondes, and meteorological analyses from the NCEP global forecast system (GFS). Each is described below.

[12] The High Resolution Dynamics Limb Sounder (HIRDLS) is a limb viewing infrared emission sounder, launched onboard the NASA Aura satellite on 15 July 2004 [*Gille et al.*, 2008]. HIRDLS uses 21 spectral channels spanning the wavelength range from 6.2 to 17.2 μm, and was designed to measure temperature-pressure profiles, the mixing ratios of many gas species (i.e., O_3, HNO_3, H_2O, NO_2, N_2O, CH_4, CFC-11, CFC-12, $ClONO_2$, N_2O_5), and cloud/aerosol extinction profiles. HIRDLS obtains approximately 5500 profiles per day and covers the latitude range 65°S to 82°N each day. HIRDLS views in the direction opposite to the spacecraft velocity, at an angle of 47° from the orbital plane on the side away from the sun. For an observer looking back along the orbital plane, HIRDLS views 47° to the left. The retrieval produces profiles along the directions of orbital track with each successive orbital tracks approximately 24.75° apart in longitude. The horizontal field of view (FOV) of HIRDLS is ~10 km cross track and ~100 km along track. The vertical FOV of HIRDLS is 1.2 km, and the vertical resolution as indicated by the averaging kernel is ~1 km.

[13] The data are retrieved over the pressure range from 400 to 0.1 hPa at 110 pressure levels. More details regarding HIRDLS data can be found in the overview by *Gille et al.* [2008]. Data products are available at the NASA GES Distributed Active Archive Center (http://disc.sci.gsfc.nasa.gov/data/datapool/). The HIRDLS validation papers used V3 data. The updated validation results are contained in the HIRDLS Data Quality Document that is available from the NASA Data and Information Services Center (DISC) at Goddard Space Flight Center, or from the HIRDLS web site http://www.eos.ucar.edu/hirdls/.

[14] Ozone profile retrieval validation [*Nardi et al.*, 2008] indicates that the ozone precision is estimated to be between 5 and 10% between 1 and 50 hPa, and comparisons with ozonesondes and lidar demonstrate that HIRDLS is capable of resolving fine vertical ozone features (1–2 km in vertical extent) between 1 and 50 hPa. Additional validation efforts for the lower altitudes (50–400 hPa) are ongoing. The version 3 product is used in this work. In our analyses, ozone profiles are screened by data precisions and vertical gradients, using criteria recommended by the HIRDLS science team.

[15] Ozonesonde data used in this study are from the World Ozone and Ultraviolet Radiation Data Center (WOUDC), operated by Environment Canada (http://www.woudc.org/). All measurements were made with

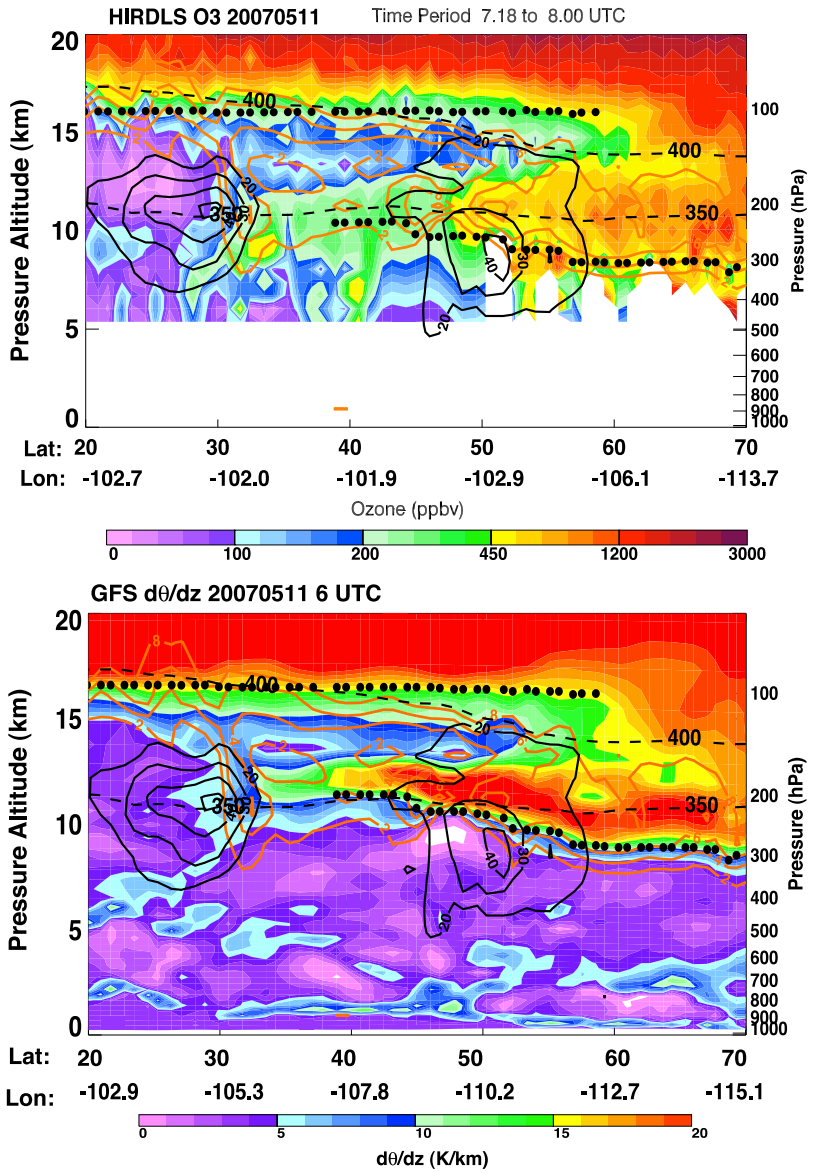

Figure 1. Cross section along the HIRDLS FOV track (shown on the map in Figure 2) on 11 May 2007. One missing profile from the ozone retrieval was filled by horizontal interpolation along the track. The layer structure of the intrusion is consistently shown in (top) the ozone cross section measured by HIRDLS and (bottom) the PTLR cross section based on the GFS analyses. The GFS analyses thermal tropopause (black dots), zonal wind (black contour), 350 and 400 K isentropes (black dashed), and PV (2, 4, 6, and 8 pvu) contours are shown on the cross sections.

ECC ozonesondes, which have a precision of 3–5% and an absolute accuracy of about 10% in the troposphere [*Smit et al.*, 2007]. Sonde response time (e^{-1}) is about 25 s, which corresponds (on the basis of a typical balloon ascent rate of 4–5 m s^{-1}) to a vertical resolution of about 100–125 m.

[16] The global meteorological analyses used in this study are based on National Centers for Environmental Prediction (NCEP) the Global Forecast System (GFS) data (http://wwwt.emc.ncep.noaa.gov/gmb/para/parabout.html). Most of the analyses used are from the 60-km resolution (T254) model run, implemented in May 2005. The data sets are provided four times daily on a 0.5° × 0.5° global grid with 47 pressure levels from 1000 to 1 hPa. More information on the data sets can be found online at http://www.emc.ncep.noaa.gov/gc_wmb/Documentation/TPBoct05/T382.TPB.FINAL.htm.

3. Spatial Extent and the Diagnostic of the Intrusion: Event of 11 May 2007

[17] During 8–13 May 2007, a large intrusion event occurred over North America. The event first developed off the west coast along the jet stream. It evolved into a larger area once it moved into the continent, covering more than 20° in latitude and much of the continental United States. The peak of the event was on 11 May. Meteorologically, the event followed the development of a large, deep ridge near the west coast of the North American

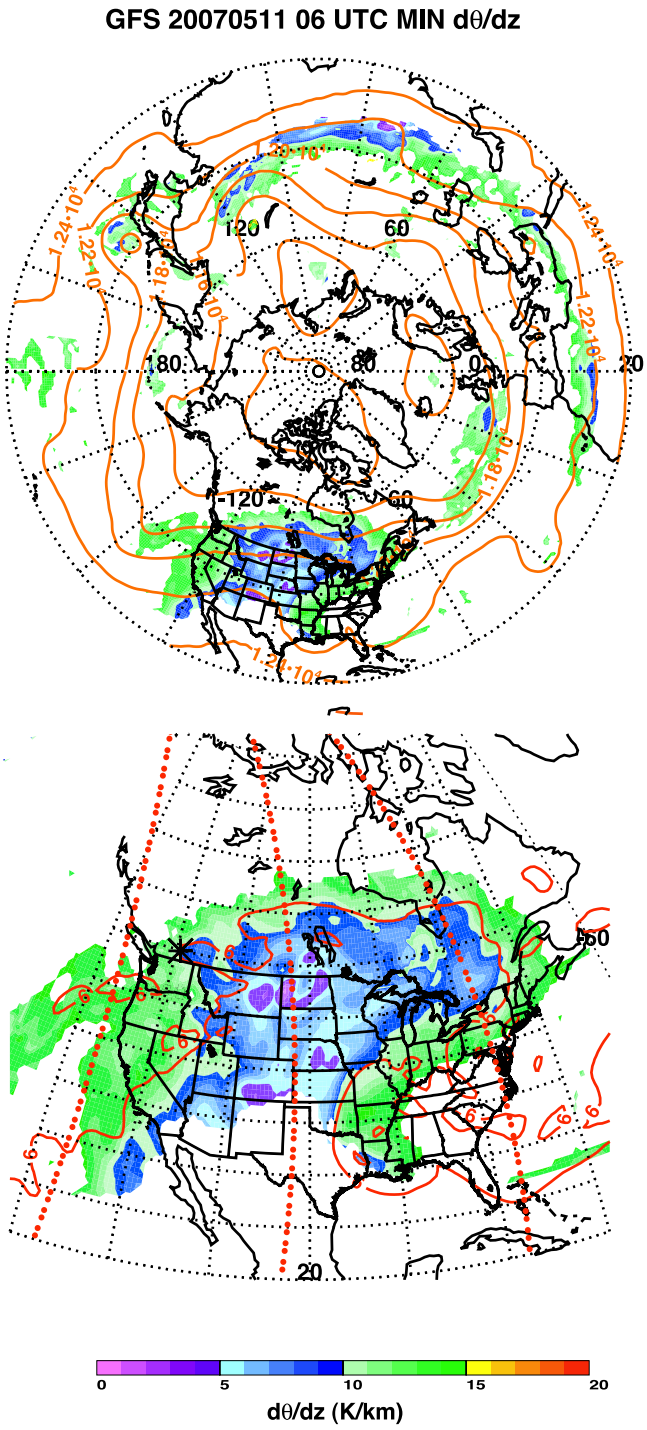

Figure 2. Region of double tropopauses on 11 May 2007. The color image represents the minimum PTLR between the primary and secondary tropopauses. Contours superimposed are (top) 200 hPa GPH and (bottom) 6 pvu PV. The red dotted lines (Figure 2, bottom) show the HIRDLS FOV tracks. The cross section of the center track is shown in Figure 1.

continent. Blocked by the ridge, the polar jet stream turned northward. The cores of both the subtropical and the polar jets were relatively low at around 250 hPa and 300 hPa, respectively. A prominent low-ozone layer near 150 hPa was observed by the HIRDLS instrument during multiple passes on both ascending and descending orbits. Shown in Figure 1 is the ozone cross section for the descending orbit on 11 May over the central United States, as indicated on the map in Figure 2. Also shown in Figure 1 is the potential temperature lapse rate (PTLR), as a measure of the air mass's static stability, for the cross section, based on the high-resolution GFS data. Superimposed on both cross sections are the thermal tropopause, zonal wind field, potential vorticity (PV) and 350 K and 400 K isentropes, also from the GFS data.

[18] The ozone cross section and the corresponding PTLR cross section have similar spatial structure. Together, they show that the layer of low-ozone and low-stability air extends into high latitudes from the subtropics, above the well-defined extratropical tropopause and a layer of high-stability air. The structure of the layer is centered near the 150 hPa pressure level, extending from 30°N to 60°N. In potential temperature, the center is around 370 K near 30°N and around 400 K near 55°N. The structure is bounded equatorward by the subtropical jet (around 30°N), and diminishes poleward over the polar jet (around 50°N). The top of the layer follows the tropical tropopause, which has extended into high latitudes and becomes the secondary tropopause over the region of 40–60°N. The minimum ozone in the center of the layer is near 100 ppbv and PTLR between 5 and 6 K/km, both similar to that of tropospheric air. In the layer, the ozone value is mostly around 100–200 ppbv, much lower than the background lower stratospheric value (greater than 400 ppbv). The core of the layer has PTLR below 10 K/km, also much lower than background stratospheric (≥15 K/km) values. Additional indication of tropospheric influence is given by the PV structure. There are several pockets of PV less than 2 pvu near the center of the layer and most of the layer is under 6 pvu.

[19] The consistency between the low-ozone layer and the low-PTLR layer between the double tropopause suggests that the intruding air mass can be located using meteorological analyses. Figure 2 maps the area of double tropopauses over the Northern Hemisphere (NH) and North America for this day using the minimum value of the PTLR between the two tropopauses. Additional meteorological variables plotted are 200 hPa GPH and the 6 pvu contour for PV at the 150 hPa level. The ground track of the HIRDLS cross section used in Figure 1 is also plotted on the map. Although not shown, the HIRDLS ozone cross sections for the orbits on the east and west side of the orbit shown in Figure 1 show similar structure for the intruding layer, further evidence for the horizontal extent of the layer indicated on the map. The horizontal map and the vertical cross section together provide a view of the 3-D structure of the intruding air mass. Note that with the exception of the region over North America, the double tropopause occurs over narrow latitude bands for most other longitudes. These bands are located near the subtropical or polar jet core, where the tropopause changes altitudes and the upper tropopause and lower tropopause tend to have a narrow overlap on the poleward side of the jet. These narrow regions of double tropopause are much more common occurrences and are consistent with the effect of the secondary meridional circulation [e.g., *Shapiro*, 1981]. Their effect of transport is limited and should be

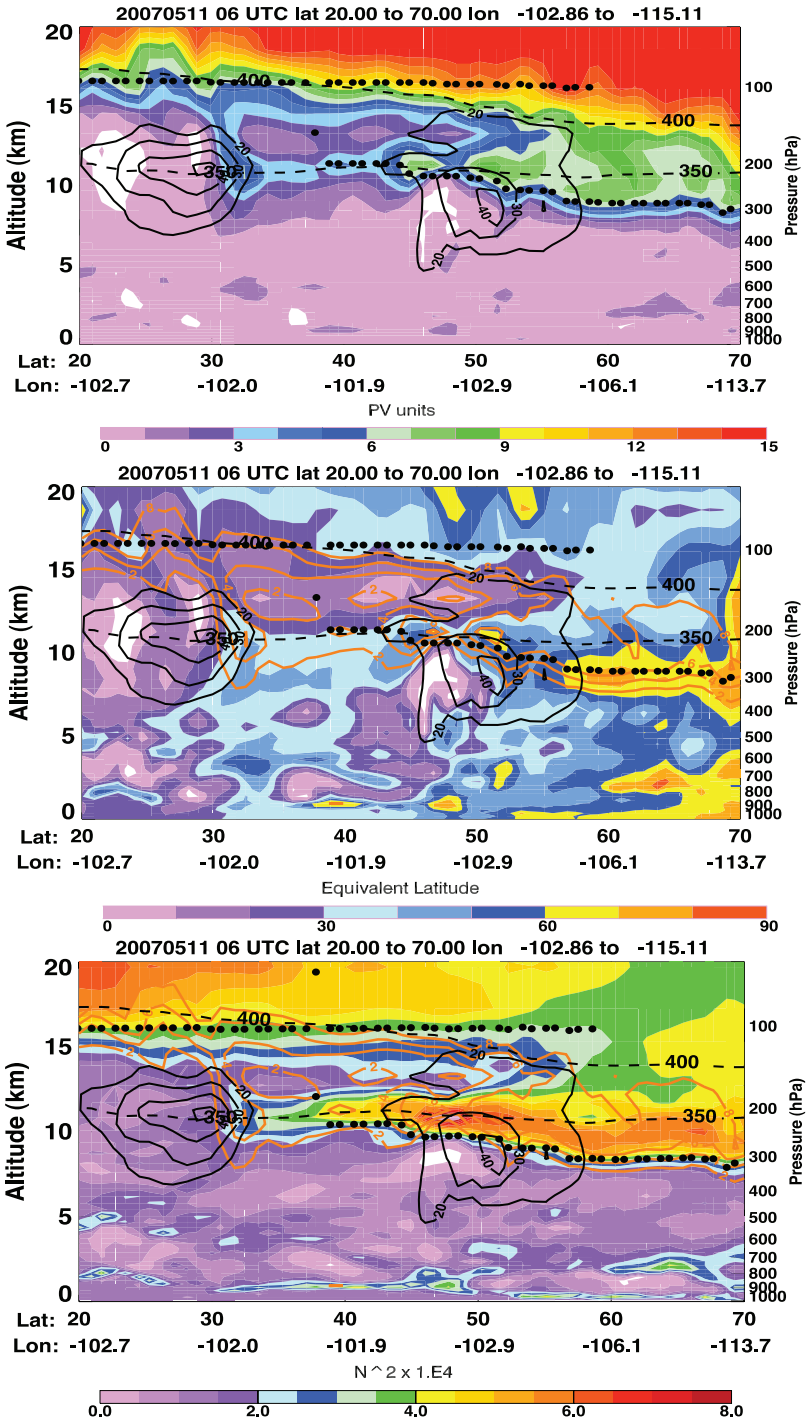

Figure 3. (top) Potential vorticity (PV), (middle) PV based equivalent latitude, and (bottom) buoyancy frequency squared (N^2) for the cross section along HIRDLS FOV track shown in Figure 1.

distinguished from the deep event shown in the region over North America.

[20] The spatial pattern similarity between HIRDLS ozone and GFS PTLR suggests that the static stability between the primary and secondary tropopause can serve as a diagnostic for the intruding air mass. The variable PTLR gives a direct quantitative measure of how stratified the region is in units of K per kilometer. In general, we find that the region with a layer of minimum PTLR below 10 K/km between the two tropopauses is always associated with low ozone, indicating tropospheric influence. This region is often associated with air mass of 6 pvu or less, but the influence of the intrusion is often not limited to these values, as indicated in the next example. Note that the static stability in this region is often the main component of PV, because the region is above the jet core and the vorticity term of PV is relatively small as a result of the weak gradient in the wind fields. There are similarities and differences between PV and static stability in revealing the tropospheric influence. Figure 3 shows cross sections of PV,

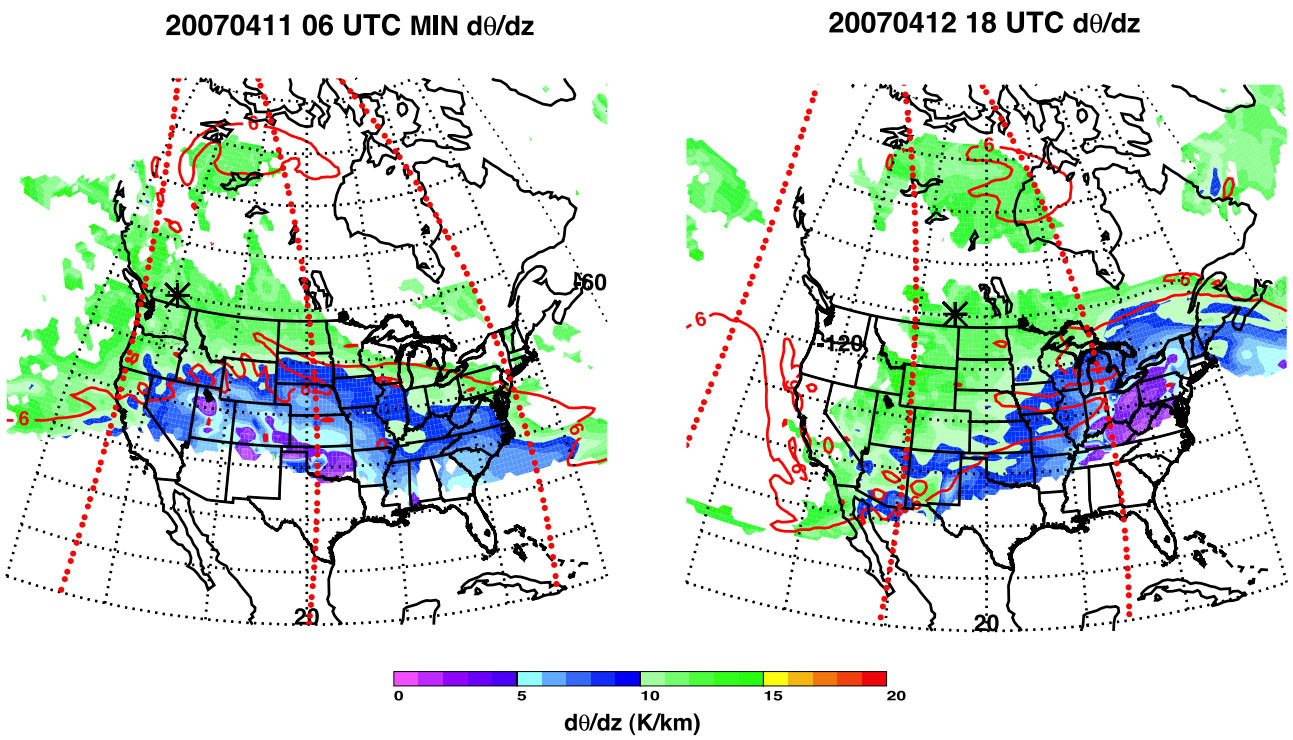

Figure 4. Map of double tropopause regions for 0600 UTC on 11 April and 1800 UTC on 12 April 2007. Shown on the map are minimum PTLR, the 6 pvu contour (red), and the HIRDLS FOV tracks (dotted red lines). The locations of two Environment Canada ozonesonde launch sites are marked by asterisks, Kelowna (49.94°N, 119.4°W) and Bratts Lake (50.2°N, 104.7°W).

PV based equivalent latitudes [e.g., *Butchart and Remsberg*, 1986; *Lait et al.*, 1990], and the buoyancy or Brunt-Vaisala frequency squared (N^2) for the same HIRDLS FOV track on 11 May 2007. The structure of the intruding layer is clearly visible in all three fields and each has somewhat different characteristics. In the PV field, the intruding air mass is associated with a structure of low-PV air between 2 and 8 pvu, normally associated with stratospheric air. The top of the layer slopes down with latitude, with the top boundary of the low-PV layer closely aligned with the 400 K level, while the ozone and PTLR field are aligned with the pressure level and the thermal tropical tropopause. Equivalent latitude is a scaled PV field, which removes the strong dependence of PV on altitude. It shows that the air mass in the layer is associated with 30° or lower equivalent latitudes, similar to the air mass on the equator flank of the subtropical jet. The buoyancy frequency squared is related to PTLR, i.e., $N^2 \sim \frac{1}{\theta}\frac{\partial\theta}{\partial z}$. In general, it provides a similar structure of the layer, but the additional inverse dependence on θ makes it less similar in spatial pattern to ozone and PTLR at high-latitude stratosphere. Overall, the PTLR diagnostic shows the best spatial similarity with the HIRDLS ozone structure, and provides a simple quantity to diagnose the intrusion.

4. Corroborative Observations and the Dynamical Evolution of the Intrusion: Event of 11 April 2007

[21] In this section we examine the dynamical evolution of the intruding air mass using a case observed in April 2007. During this time period, in addition to HIRDLS ozone retrievals, there are ozonesonde profiles that sampled the same event, capturing the ozone minimum between the primary and secondary tropopauses. These measurements are used to validate the structure observed in the satellite data, and additionally the structure of the intruding layer is mapped out using meteorological analyses.

[22] Figure 4 displays maps of the double tropopause region over North America and the minimum PTLR for two times, 0600 UT on 11 April and 1800 UT on 12 April. These two maps, 36 h apart, give a perspective to the relatively slow evolution of the feature over the period. They also provide connections between the measurements that sampled this event at different times and locations. The HIRDLS tracks and the ozonesonde launch sites are marked on the maps. The vertical extent of the intruding layer is shown in Figure 5 using the collocated HIRDLS ozone and GFS PTLR cross sections for the orbit over the central United States on 11 April.

[23] Figure 6 shows two ozone profiles around 50°N for 11 and 12 April showing a pronounced layer of low ozone centered near 15 km. Several HIRDLS profiles from a nearby track are selected for comparisons. The comparisons show that the HIRDLS ozone captured the ozone minimum and the structure of the low-ozone layer, despite substantial uncertainties at the altitudes below the layer.

[24] One of the most interesting aspects of this case is the region of anomalous low ozone observed by the HIRDLS cross section at high latitude (near 65°N), which is spatially colocated with a region of low-stability air shown in the GFS PTLR cross section. This particular air mass (ozone

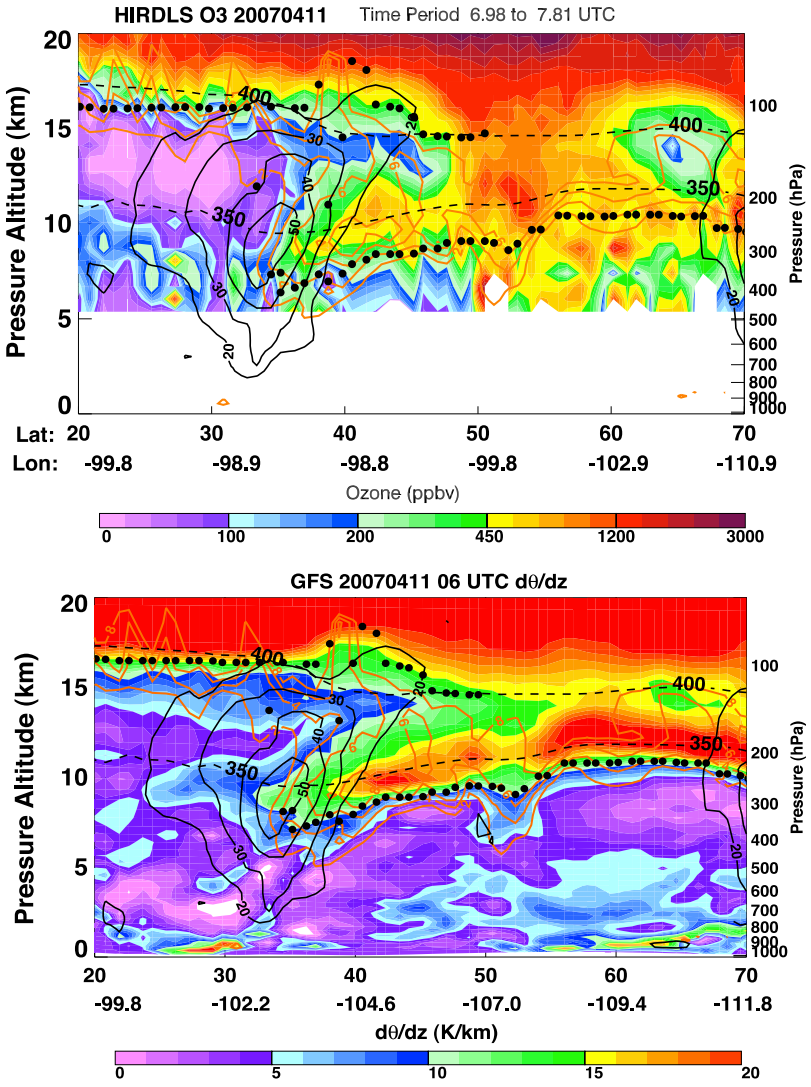

Figure 5. Cross sections of HIRDLS ozone for the 11 April 2007 along the central U.S. descending FOV track (marked on the map in Figure 4) and the corresponding PTLR cross section from GFS. Six missing profiles are filled in the ozone cross section. The ground track of the cross section is marked on the map in Figure 4.

minimum ~ 100 ppbv) can be found in Figure 4 near 60°N, 120°W on the map for 11 April and is within the contour of 6 pvu. The cross section in Figure 5 shows clearly that the low-stability layer in this case extends beyond the continuous double tropopause region. This event provides a good case for investigating the 3-D structure of the intruding air mass in the context of its dynamical evolution.

[25] The evolution is investigated using parcel back trajectories (Figure 7). Ten-day back trajectories for two groups of air parcels are calculated using the CLAMS model [*McKenna et al.*, 2002]. Parcels are initiated in the 13–16 km vertical range on 7 evenly spaced levels with 1° increments in latitude along the FOV track. The first group corresponds to the location of anomalous low ozone on the cross section in Figure 5, initiated in latitude 60–67°N. The second group covers latitudes 50–57°N, corresponding to the section with high or normal stratospheric ozone values (~1 ppmv). The two groups of parcels clearly have different origins: of the group with anomalous low ozone (green), all originate from tropical/subtropical latitudes and have followed very similar paths, while of the group with ozone amounts typical of the lower stratosphere, all originate from higher latitudes and have moved (less coherently) to similar or lower latitudes.

[26] To relate the parcel's motion to the background meteorology, Figure 8 shows 4 snapshots of the parcels' positions and the corresponding meteorological fields (GPH, jet locations and 2 and 4 pvu contours) at four different times. The snapshots indicate that the event is associated with the growth and decay of a classical omega shaped blocking ridge over North America, which began to develop ~6 days before the observation. Parcels of anomalously low ozone were in tropical/subtropical latitudes (20–30°N) over south Asia around 6 days before the observation, began a northward excursion along the ridge ~4 days before the observations and experienced RWB ~ 1 day before the observation when a blocking high formed around the Arctic circle in the center of the omega.

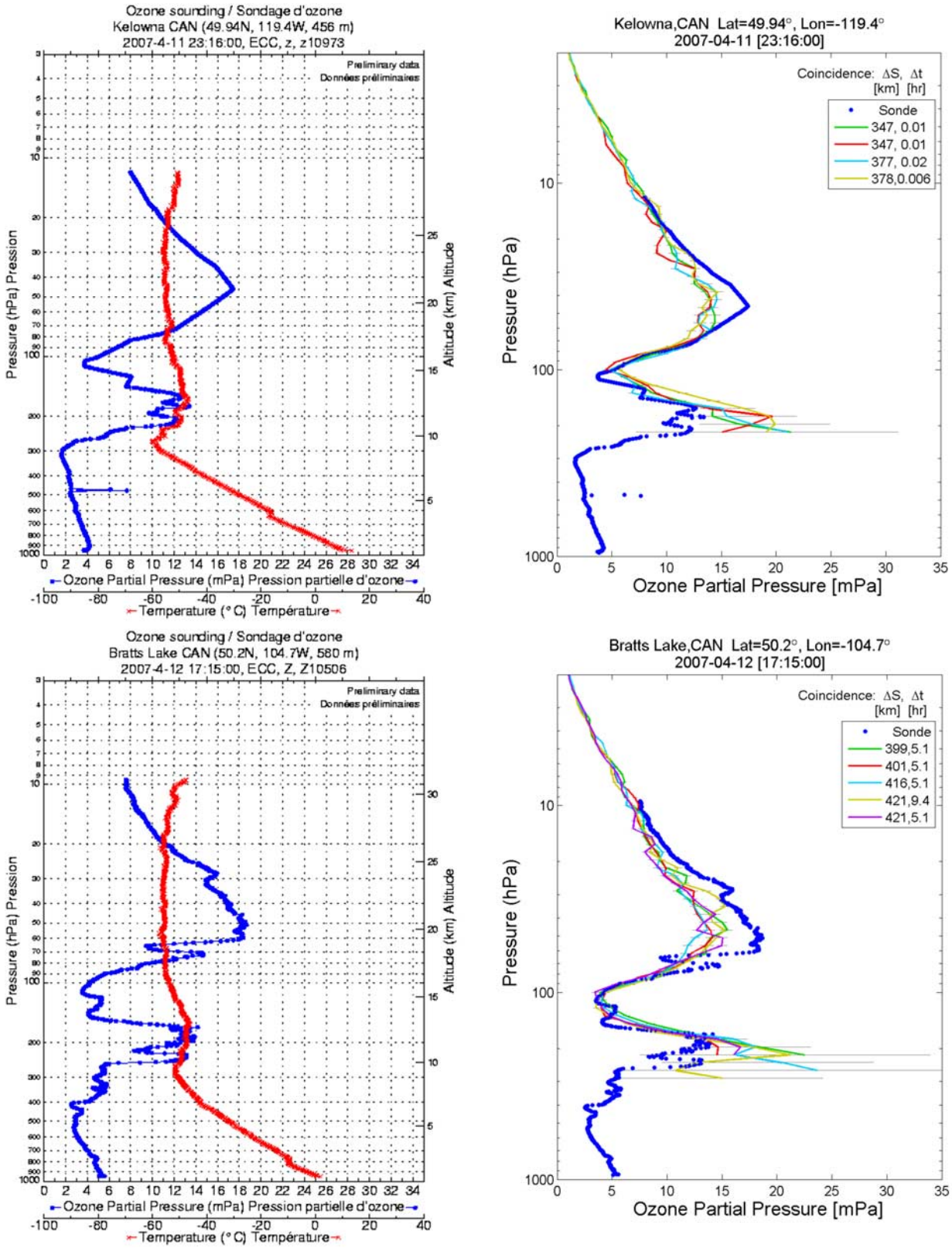

Figure 6. The low-ozone layer above the first tropopause associated with the intrusion captured by the ozonesonde profile from the Environment Canada stations at Kelowna (49.94°N, 119.4°W) on 11 April and Bratts Lake (50.2°N, 104.7°W) on 12 April 2007. (left) Ozone (blue curve) and temperature (red curve) profiles reported by the stations. (right) Comparisons of HIRDLS ozone profiles in a nearby track with the ozonesonde profiles. The light gray lines indicate the retrieval uncertainties. The spatial and temporal distances between the sonde and HIRDLS samplings are given in the legend.

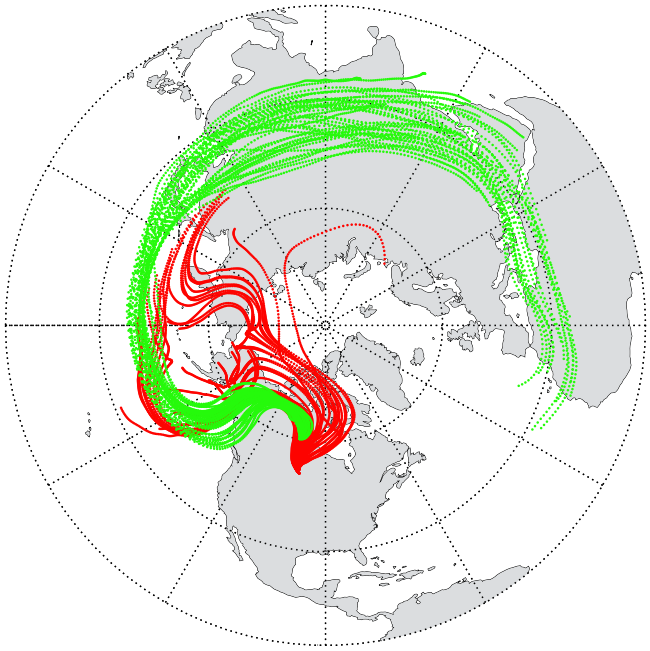

Figure 7. The 10-day back trajectories of air mass along the HIRDLS cross section, as shown in Figure 5. Parcels in green are initiated in the region 60–67°N, 13–16 km, corresponding to the low-ozone air mass. Parcels in red are initiated for the same altitude range but between 50 and 57°N, corresponding to the high-ozone air mass.

The wave breaking is indicated by the overturning of high ozone and low-ozone air masses in their relative latitudes. These dynamical evolutions were similar to that discussed by *Vaughan and Timmis* [1998]. While the overturning of the two groups is a result of the poleward wave breaking, the 2 and 4 pvu contours are showing equatorward wave breaking during the same time period. An animated version of Figure 8 for the 10-day period is included in the auxiliary material.[1]

[27] The RWB event is clearly represented in the 150 hPa PV field, shown in Figure 9. The low-ozone air mass near the Canadian Arctic circle is associated with a region of low-PV air mass (pv < 6 pvu) (northwest of 60°N and 90°W), which is north of an air mass with higher PV (9–10 pvu). This wave-breaking feature can be seen in the PV field over a range of isentropes from 360K to 390K (not shown). Comparing this with the minimum PTLR map given in Figure 9, it is interesting how the two fields complement each other in providing perspectives of the wave breaking and its particular consequence. While the PV field shows the reversal of gradient as an indication of wave breaking [e.g., *Postel and Hitchman*, 1999], the PTLR in the double tropopause field shows the region of deep tropospheric intrusion into high latitude as the consequence. An additional region of double tropopauses at high latitude is shown on the map in the Arctic region over northern Europe, corresponding to a similar poleward wave breaking event shown in the PV map. Both events are associated with the growth and decay of a ridge structure in the diffluence region as discussed by *Peters and Waugh* [1996]. An animation of the fields shown in Figure 9 over this time period is also included in the auxiliary material.

5. Discussion and Conclusions

[28] We have examined two cases of the intrusion of subtropical tropospheric air deep into the lower stratosphere. These cases were selected to demonstrate the relationship of the intrusion and the secondary tropopause, the 3-D spatial extent of such events, as well as the origin and the evolution of the intruding air. These selected cases are not isolated events but a subset of a much larger collection of events evident in ozone and PTLR fields. Quantifying the frequency of occurrence of the low-ozone layer is a topic of ongoing research. From our initial examination, these structures exist in ~20% of the HIRDLS profiles over NH midlatitudes during winter-spring. Previous ozonesonde data analyses show that the type of event contributes to approximately 10–15% decrease in the ozone total column [*Reid et al.*, 2000]. How they impact the overall ozone budget is a subject of future study.

[29] The ozone observations combined with the meteorological analyses present clear evidence that the secondary tropopause as defined by the thermal definition has a clear physical interpretation. The secondary tropopause that extends from the subtropical tropopause break is a manifestation of the transport of subtropical air into the high-latitude lower stratosphere, bringing low ozone and associated tropospheric air. The secondary extratropical tropopause under these conditions is the physical boundary of two distinct air masses above and below. The fact that double tropopauses are frequently observed in midlatitudes, plus the frequent occurrence of these events in HIRDLS ozone observations suggests these intrusions may be a persistent feature of the UTLS region. These likely contribute to the ventilation of the lower stratosphere above the subtropical jet, as discussed by *Berthet et al.* [2007].

[30] The low-ozone layer is also characterized by low static stability, which is additional evidence of its origin in the subtropical upper troposphere. The static stability structure between the primary and secondary extratropical tropopause, therefore, serves to identify the region influenced by transport. The PTLR between the two tropopauses provides a diagnostic for identifying the region of tropospheric influence in the lower stratosphere. The observed low-ozone layer between the primary and secondary tropopause is found to be associated with PTLR below 15 K/km, while the background stratosphere is represented by PTLR greater than 15 K/km. Although static stability is not a conservative quantity, it is a key dynamical variable, especially for the air mass of tropical tropospheric origin.

[31] The intruding layer is also characterized by relatively low PV values and is particularly evident using PV-based equivalent latitude (Figure 3, middle). In the region of interest, PTLR is often the main component of PV. Since these events are occurring at higher isentropes than most previous STE studies, where the focus is often on 320–360 K and 2–4 pvu range [e.g., *Appenzeller et al.*, 1996; *Postel and Hitchman*, 1999; *Dethof et al.*, 2000; *Sprenger et*

[1] Auxiliary materials are available in the HTML. doi:10.1029/2008JD011374.

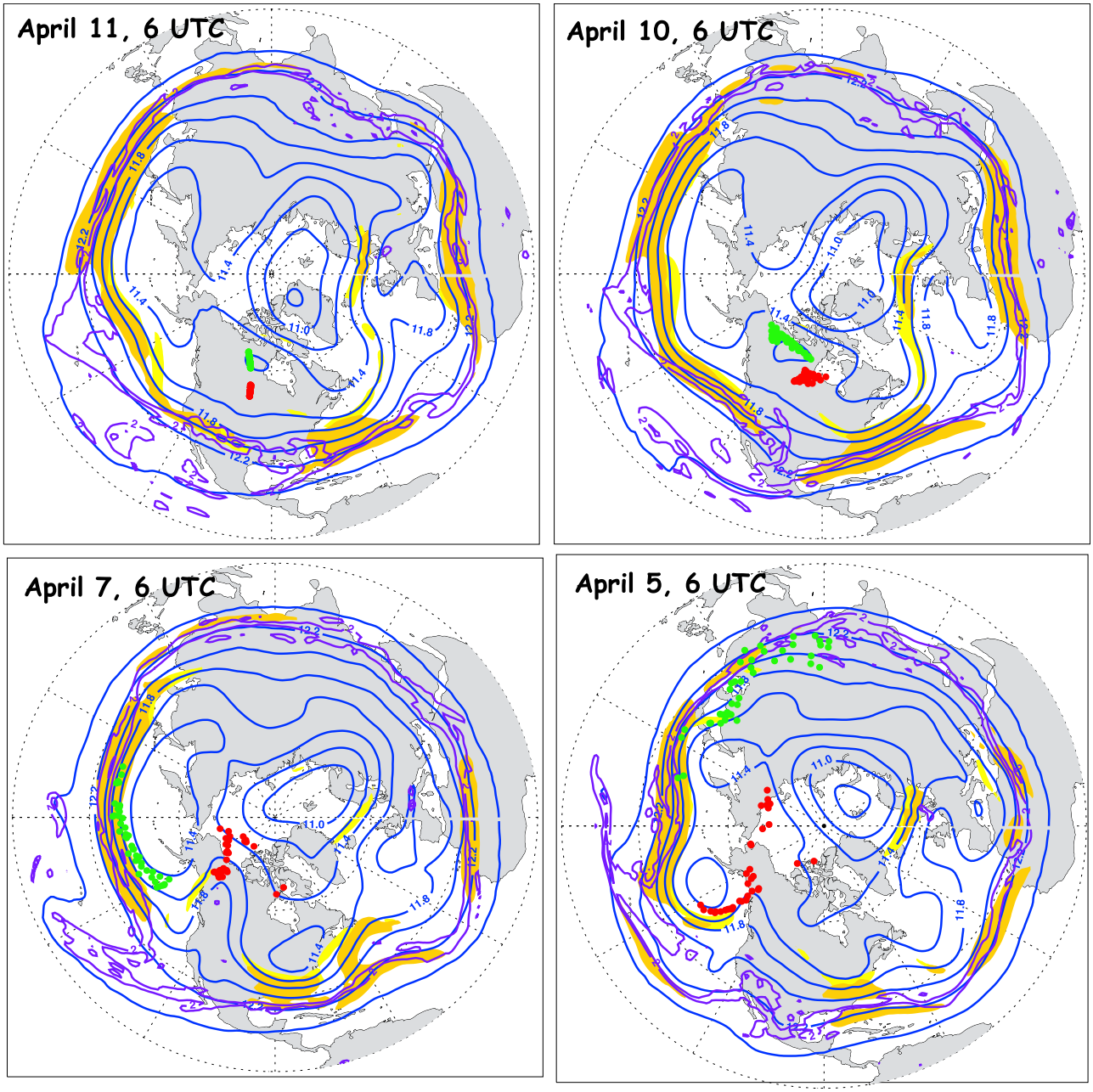

Figure 8. History of air parcels and corresponding meteorological fields at four time steps for the observations of 11 April 2007 (Figure 8). The 200 hPa GPH is shown in blue contours. The 150 hPa PV (2 and 4 pvu) are shown in purple. The 300 and 200 hPa horizontal wind (50 m/s) are shown in lighter and darker yellow shadings. Parcels from the region of observed anomalous low ozone (60–67°N, 150–200 hPa) are in green. Parcels from the adjacent region (50–57°N) with normal lower stratospheric ozone are in red.

al., 2007], the range of PV values of interest is also higher. We found that the relatively low PV could be as high as 8 pvu using Ertel's definition. The specific value or range of PV that can be used to identify the intrusion event varies with the potential temperature level of the intrusion. The PV-based equivalent latitude may be a more effective diagnostic.

[32] Consistent with previous studies [*Vaughan and Timmis*, 1998; *O'Connor et al.*, 1999], our case study from April 2007 indicates that the intrusion events were associated with RWB. In this case the poleward RWB brought low-stability air and resulted in the thermal structure for the high-latitude double tropopause. This suggests that RWB is an important process for producing the double tropopause. The dynamical behavior of the RWB has been previously investigated largely for lower isentropes. How similar or different it is in the 370–420 K range and its seasonal variation deserves future investigation. In addition, a model study of long-range troposphere-to-stratosphere transport by large synoptic-scale waves by *Rood et al.*

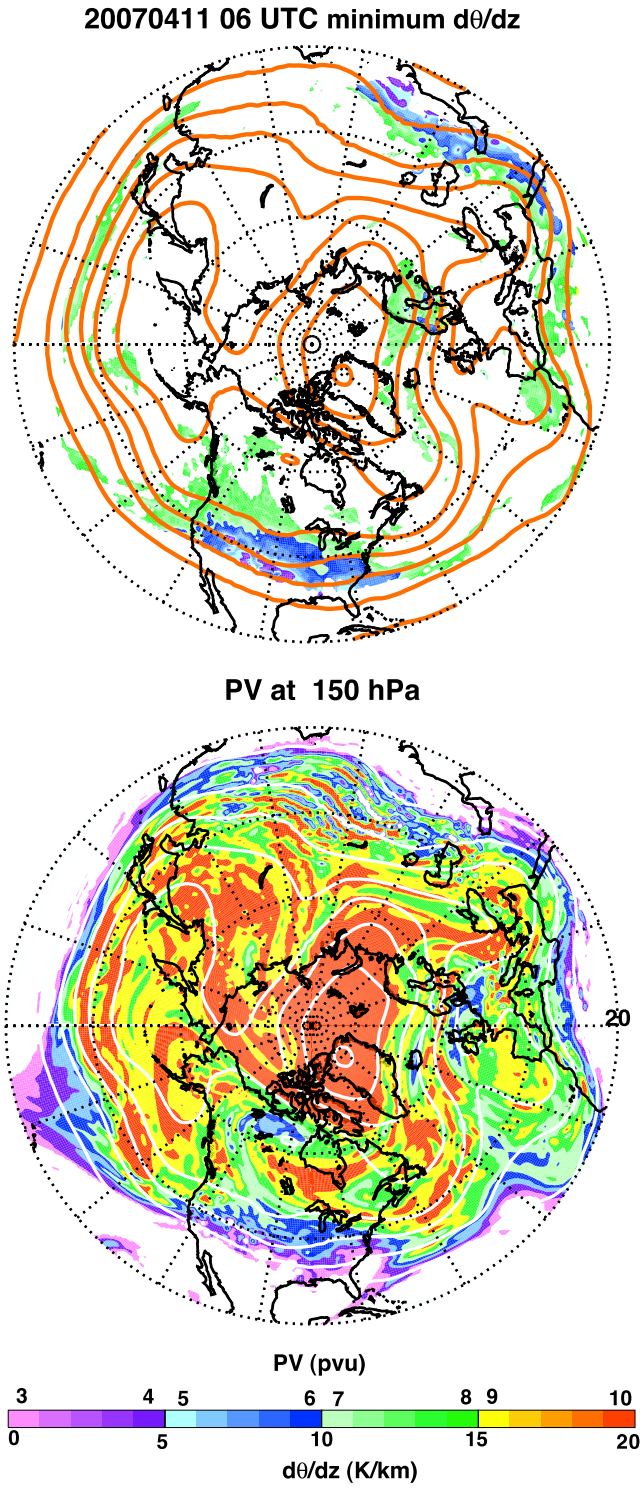

Figure 9. Map of the low-stability layer between the double tropopause and PV for the 11 April event. Wave breaking that led to the low-ozone air mass in the HIRDLS cross section can be seen in the PV map, ~6 pvu air mass (blue) over northern Canada.

[1997] shows that thermodynamic processes are important if these processes result in irreversible transport. Since this type of event will alter the composition of the lowermost stratosphere in a significant fashion, it is important to understand the mechanism that controls its occurrence and how it may respond to a future changing circulation pattern.

[33] Although not a focus of this analysis, the low-stability layer brought to the middle- to high-latitude region by transport alters the thermal structure of the lowermost stratosphere. This is of interest to the issue of the tropopause inversion layer (TIL), a layer of high static stability right above the tropopause identified from high-resolution temperature profile analyses [*Birner*, 2006, and references therein]. In fact, such an inversion layer above the extra-tropical tropopause is often observed in association with the intrusion events (see Figure 3 and the temperature profiles in Figure 6). It is not yet clear if the inversion layer, which exhibits higher stability than the stratosphere above, is controlled by dynamics or radiation [*Randel et al.*, 2007b]. The transport process discussed in this work contribute to the lower static stability above the inversion layer, but the links to the TIL itself are not clear. The role of intrusion dynamical processes in the formation of the TIL deserves further study.

[34] The use of PTLR between the double tropopause as a diagnostic not only facilitated identification of occurrences of low-ozone layers in the HIRDLS data, but also enabled forecasting of intrusion events for field studies and led to successful aircraft investigations during the Stratosphere-Troposphere Analyses of Regional Transport (START08) field campaign in spring 2008. These results will be reported in the near future.

[35] **Acknowledgment.** The National Center for Atmospheric Research is sponsored by the National Science Foundation.

References

Appenzeller, C., H. C. Davies, and W. A. Norton (1996), Fragmentation of stratospheric intrusions, *J. Geophys. Res.*, *101*, 1435–1456, doi:10.1029/95JD02674.

Berthet, G., J. G. Esler, and P. H. Haynes (2007), A Lagrangian perspective of the tropopause and the ventilation of the lowermost stratosphere, *J. Geophys. Res.*, *112*, D18102, doi:10.1029/2006JD008295.

Birner, T. (2006), Fine-scale structure of the extratropical tropopause region, *J. Geophys. Res.*, *111*, D04104, doi:10.1029/2005JD006301.

Butchart, N., and E. E. Remsberg (1986), The area of the stratospheric polar vortex as a diagnostic for tracer transport on an isentropic surface, *J. Atmos. Sci.*, *43*, 1319–1339, doi:10.1175/1520-0469(1986)043<1319:TAOTSP>2.0.CO;2.

Danielsen, E. F. (1968), Stratospheric-tropospheric exchange based on radioactivity, ozone and potential vorticity, *J. Atmos. Sci.*, *25*, 502–518, doi:10.1175/1520-0469(1968)025<0502:STEBOR>2.0.CO;2.

Dethof, A., A. O'Neill, and J. Slingo (2000), Quantification of the isentropic mass transport across the dynamical tropopause, *J. Geophys. Res.*, *105*(D10), 12,279–12,293, doi:10.1029/2000JD900127.

Dobson, G. M. B. (1973), The laminated structure of the ozone in the atmosphere, *Q. J. R. Meteorol. Soc.*, *99*, 599–607, doi:10.1002/qj.49709942202.

Gille, J., et al. (2008), High Resolution Dynamics Limb Sounder: Experiment overview, recovery, and validation of initial temperature data, *J. Geophys. Res.*, *113*, D16S43, doi:10.1029/2007JD008824.

Holton, J. R., P. H. Haynes, M. E. McIntyre, A. R. Douglass, R. B. Rood, and L. Pfister (1995), Stratosphere-troposphere exchange, *Rev. Geophys.*, *33*, 403–439, doi:10.1029/95RG02097.

Hoskins, B. J. (1991), Towards a PV-theta view of the general circulation, *Tellus, Ser. A*, *43*, 27–35.

Hoskins, B. J., M. E. Mcintyre, and N. Robertson (1985), On the use and significance of isentropic potential vorticity maps, *Q. J. R. MeteoroI. Soc.*, *111*, 877–946, doi:10.1256/smsqj.47001.

Hwang, S.-H., J. Kim, and G.-R. Cho (2007), Observation of secondary ozone peaks near the tropopause over the Korean peninsula associated with stratosphere-troposphere exchange, *J. Geophys. Res.*, *112*, D16305, doi:10.1029/2006JD007978.

Kochanski, A. (1955), Cross sections of the mean zonal flow and temperature along 80°W, *J. Meteorol.*, *12*, 95–106.

Lait, L. R., et al. (1990), Reconstruction of O_3 and N_2O fields from ER-2, DC-8, and balloon observations, *Geophys. Res. Lett.*, *17*, 521–524, doi:10.1029/GL017i004p00521.

Lemoine, R. (2004), Secondary maxima in ozone profiles, *Atmos. Chem. Phys.*, *4*, 1085–1096.

McKenna, D. S., P. Konopka, J.-U. Grooß, G. Günther, R. Müller, R. Spang, D. Offermann, and Y. Orsolini (2002), A new Chemical Lagrangian Model of the Stratosphere (CLaMS): 1. Formulation of advection and mixing, *J. Geophys. Res.*, *107*(D16), 4309, doi:10.1029/2000JD000114.

Nardi, B., et al. (2008), Initial validation of ozone measurements from the High Resolution Dynamics Limb Sounder, *J. Geophys. Res.*, *113*, D16S36, doi:10.1029/2007JD008837.

O'Connor, F. M., G. Vaughan, and H. de Backer (1999), Observations of subtropical air in the European mid-latitude lower stratosphere, *Q. J. R. Meteorol. Soc.*, *125*, 2965–2986, doi:10.1256/smsqj.56008.

Olsen, M. A., A. R. Douglass, P. A. Newman, J. C. Gille, B. Nardi, V. A. Yudin, D. E. Kinnison, and R. Khosravi (2008), HIRDLS observations and simulation of a lower stratospheric intrusion of tropical air to high latitudes, *Geophys. Res. Lett.*, *35*, L21813, doi:10.1029/2008GL035514.

Palmen, E., and C. W. Newton (1969), *Atmospheric Circulation Systems: Their Structure and Physical Interpretation*, Academic, New York.

Peters, D., and D. W. Waugh (1996), Influence of barotropic shear on the poleward advection of upper tropospheric air, *J. Atmos. Sci.*, *53*, 3013–3031, doi:10.1175/1520-0469(1996)053<3013:IOBSOT>2.0.CO;2.

Postel, G. A., and M. H. Hitchman (1999), A climatology of Rossby wave breaking along the subtropical tropopause, *J. Atmos. Sci.*, *56*, 359–373, doi:10.1175/1520-0469(1999)056<0359:ACORWB>2.0.CO;2.

Randel, W. J., D. J. Seidel, and L. L. Pan (2007a), Observational characteristics of double tropopauses, *J. Geophys. Res.*, *112*, D07309, doi:10.1029/2006JD007904.

Randel, W. J., F. Wu, and P. Forster (2007b), The extratropical tropopause inversion layer: Global observations with GPS data, and a radiative forcing mechanism, *J. Atmos. Sci.*, *64*, 4489–4496, doi:10.1175/2007JAS2412.1.

Reid, S. J., A. F. Tuck, and G. Kiladis (2000), On the changing abundance of ozone minima at northern midlatitudes, *J. Geophys. Res.*, *105*(D10), 12,169–12,180, doi:10.1029/2000JD900081.

Rood, R., A. Douglass, M. Cerniglia, and W. Read (1997), Synoptic-scale mass exchange from the troposphere to the stratosphere, *J. Geophys. Res.*, *102*(D19), 23,467–23,485, doi:10.1029/97JD01598.

Schmidt, T., G. Beyerle, S. Heise, J. Wickert, and M. Rothacher (2006), A climatology of multiple tropopauses derived from GPS radio occultations with CHAMP and SAC-C, *Geophys. Res. Lett.*, *33*, L04808, doi:10.1029/2005GL024600.

Seidel, D. J., and W. J. Randel (2006), Variability and trends in the global tropopause estimated from radiosonde data, *J. Geophys. Res.*, *111*, D21101, doi:10.1029/2006JD007363.

Shapiro, M. A. (1978), Further evidence of the mesoscale and turbulent structure of upper level jet stream–frontal zone systems, *Mon. Weather Rev.*, *106*, 1100–1110, doi:10.1175/1520-0493(1978)106<1100:FEOTMA>2.0.CO;2.

Shapiro, M. A. (1981), Frontogenesis and geostrophically forced secondary circulations in the vicinity of jet stream-frontal zone systems, *J. Atmos. Sci.*, *38*, 954–973, doi:10.1175/1520-0469(1981)038<0954:FAGFSC>2.0.CO;2.

Smit, H. G. J., et al. (2007), Assessment of the performance of ECC-ozonesondes under quasi-flight conditions in the environmental simulation chamber: Insights from the Juelich Ozone Sonde Intercomparison Experiment (JOSIE), *J. Geophys. Res.*, *112*, D19306, doi:10.1029/2006JD007308.

Sprenger, M., H. Wernli, and M. Bourqui (2007), Stratosphere–troposphere exchange and its relation to potential vorticity streamers and cutoffs near the extratropical tropopause, *J. Atmos. Sci.*, *64*, 1587–1602, doi:10.1175/JAS3911.1.

Vaughan, G., and C. Timmis (1998), Transport of near-tropopause air into the lower midlatitude stratosphere, *Q. J. R. Meteorol. Soc.*, *124*, 1559–1578, doi:10.1002/qj.49712454910.

J. C. Gille, W. D. Hall, R. Khosravi, S. Massie, B. Nardi, L. L. Pan, W. J. Randel, and V. Yudin, National Center for Atmospheric Research, Boulder, CO 80305, USA. (liwen@ucar.edu)

P. Konopka, Forschungszentrum Jülich, D-52425 Jülich, Germany.

D. Tarasick, Experimental Studies, Air Quality Research Division, Environment Canada, 4905 Dufferin Street, Downsview, ON M3H 5T4, Canada.